

# Normal form expansions and thermal decay rates of Bose-Einstein condensates with short- and long-range interaction

Andrej Junginger,\* Teresa Schaller, Gela Hämmerling, Jörg Main, and Günter Wunner  
*Institut für Theoretische Physik 1, Universität Stuttgart, 70550 Stuttgart, Germany*

(Dated: December 7, 2024)

The thermally induced coherent collapse of Bose-Einstein condensates at finite temperature is the dominant decay mechanism near the critical scattering length in condensates with at least partially attractive interaction. The collapse dynamics out of the ground state is mediated by a transition state whose properties determine the corresponding decay rate or lifetime of the condensate. In this paper, we perform normal form expansions of the ground and the transition state of condensates with short-range scattering interaction as well as with anisotropic and long-range dipolar interaction in a variational framework. This method allows one to determine the local properties of these states, i. e. their mean-field energy, their normal modes, the coupling between different modes, and the structure of the reaction channel to any desired order. We discuss the physical interpretation of the transition state as a certain density distribution of the atomic cloud and the behavior of the single normal form contributions in dependence on the s-wave scattering length. Moreover, we investigate the convergence of the local normal form when using extended Gaussian variational approaches, and present the condensate’s decay rate.

PACS numbers: 67.85.De, 03.75.Kk

## I. INTRODUCTION

Starting from their first experimental realization in 1995 [1–3], the field of Bose-Einstein condensates (BECs) has grown rapidly and it is the subject of numerous experimental and theoretical investigations today. By far, most of today’s experiments are performed on such macroscopic quantum objects made of alkali metals, in which the interaction between the single bosons is the short-range, spherically symmetric, low-energy s-wave scattering. Beyond these, also BECs with an additional long-range and anisotropic dipole-dipole interaction (DDI) have been realized experimentally [4–6], which are of great interest, because the interaction between two bosons depends on their relative orientation. As a consequence, interesting phenomena have been predicted in dipolar BECs, such as isotropic as well as anisotropic solitons [7–9], biconcave or structured ground state density distributions [10–12], stability diagrams that depend on the trap geometry [13–15], radial and angular rotons [11, 16, 17], and anisotropic collapse dynamics [18, 19].

If the particle interaction between the single bosons in the condensate is (at least partially) attractive, its ground state is metastable and several mechanisms can contribute to the decay of the atomic cloud. These include e. g. inelastic three-body collisions, macroscopic quantum tunneling [20, 21], the decrease of the s-wave scattering length below its critical value [11], or dipolar relaxation [22].

Another important decay mechanism is the thermally induced coherent collapse of the condensate [23–28]. This

process is based on the fact that quasi-particle excitations in a BEC at finite temperature  $T > 0$  lead to time-dependent density fluctuations of the gas. If the particle interaction is attractive, these fluctuations can induce the collapse of the condensate, when the density locally becomes high enough so that the attraction can no longer be compensated by the quantum pressure. This process is important near the critical scattering length where the attraction between the bosons becomes dominant, and it is mediated by a transition state. The latter is a collectively excited, stationary state of the condensate which typically exhibits a locally increased density in some region and which emerges together with the ground state in a tangent bifurcation at a critical value of the scattering length. The thermally induced collapse dynamics is then of the type “reactants  $\rightarrow$  transition state  $\rightarrow$  products”, so that the condensate’s decay rate or lifetime, respectively, can be calculated by applying transition state theory (TST) [29–32]: With respect to the BEC’s ground state the transition state forms an energy barrier that needs to be crossed in order to induce the collapse. Finally, the height of the energy barrier together with the local properties of the ground and the transition state determine the reaction dynamics.

A suitable theoretical framework in which the transition state is easily accessible is that of a variational approach to the Gross-Pitaevskii equation (GPE) by which the condensate is described. In this framework, the transition state is a fixed point of the corresponding dynamical equations, and its local properties are determined by the latter’s series expansion. A particularly appropriate set of coordinates into which this expansion can be transformed are its normal form coordinates. These have the advantage that locally they can be chosen as classical canonical coordinates [33], in which the condensate’s mean-field energy functional serves as a classical

---

\* andrej.junginger@itp1.uni-stuttgart.de

Hamilton function that fully describes the dynamics of the BEC. The complete information about the transition state can then be extracted from the expansion coefficients of this Hamiltonian.

In this paper, we focus on the normal form expansions of both the ground and the transition state of BECs with short-range interaction [34] as well as with long-range and anisotropic DDI [35]. We present the physical interpretation of the transition state as a certain density distribution of the atomic cloud. Moreover, we discuss the behavior of the single expansion coefficients which describe the fixed point energies, the corresponding elementary excitations and the coupling between the different normal modes. Finally, we calculate the decay rate of the condensate at experimentally relevant temperatures.

For this purpose, our paper is organized as follows: In Sec. II we discuss the theoretical description of the BEC in a variational framework, for which we introduce the GPE and a time-dependent variational principle. Moreover, we review the construction of the local normal form Hamiltonian and, with it, the calculation of the decay rate by applying TST. In Sec. III, we present the results for BECs with short-range scattering interaction as well as with long-range and anisotropic DDI.

## II. THEORY

### A. BECs at ultracold temperatures

At ultra-cold temperatures, the dynamics of a BEC is determined by the GPE (units given below)

$$i\frac{\partial}{\partial t}\psi(\mathbf{r},t) = \hat{H}\psi(\mathbf{r},t) = \left(-\Delta + V_{\text{ext}} + V_c + V_{\text{lr}}\right)\psi(\mathbf{r},t). \quad (1)$$

Here,  $V_{\text{ext}}$  is an external trapping potential, the contact interaction  $V_c = 8\pi aN |\psi(\mathbf{r},t)|^2$  describes low-energy collisions between the bosons via the s-wave scattering length  $a$  and the particle number  $N$ , and  $V_{\text{lr}}$  is a possible long-range particle interaction.

In case of a BEC without long-range interaction ( $V_{\text{lr}} = 0$ ) the internal symmetry of the system is spherical and we, therefore, also choose a spherically symmetrical external trapping potential  $V_{\text{ext}} = \frac{m}{2}\omega^2\mathbf{r}^2$ . The form of the GPE (1) with the given interaction potentials is then obtained by using the oscillator length  $r_0 = \sqrt{\hbar/m\omega}$  as a natural unit of length, with  $m$  being the mass of the bosons and  $\omega$  being the trap frequency. Natural energy and time scales are then given by  $E_0 = \hbar\omega/2$  and  $t_0 = \hbar/E_0$ . Furthermore, we use  $m_0 = 2m$  as a unit of mass.

In case of a BEC with long-range and anisotropic DDI in which all dipoles are aligned in  $z$ -direction by an external magnetic field, the long-range part of the interaction

potential in the GPE reads

$$V_{\text{lr}} = a_{\text{dd}}N \int d^3r' \frac{1 - 3\cos^2\theta}{|\mathbf{r} - \mathbf{r}'|^3} |\psi(\mathbf{r}',t)|^2. \quad (2)$$

The alignment of the dipoles naturally induces a cylindrical symmetry to the BEC and we, therefore, adapt the symmetry of the external trap to  $V_{\text{ext}} = \rho^2 + \lambda^2 z^2$  where  $\rho^2 = x^2 + y^2$ . As a length scale we use the radial oscillator length  $r_0 = \sqrt{\hbar/m\omega_\rho}$ , and we define the trap strength in  $z$ -direction via the trap aspect ratio  $\lambda = \omega_z/\omega_\rho$ . In these units, the strength of the DDI reads  $a_{\text{dd}} = \mu_0\mu^2m/(2\pi\hbar^2r_0)$  with  $\mu$  being the magnetic moment of the atoms.

### B. Time-dependent variational approach

Common methods to solve the GPE (1) are e.g. its direct numerical integration or the discretization of the wave function on grids. The condensate's dynamics and its ground state can then be calculated by applying the split-operator method and an imaginary-time evolution. As already mentioned above, a more suitable framework for the purposes of this paper is the description within a variational approach. Therein, the GPE is solved approximately by replacing the original wave function  $\psi(\mathbf{r},t)$  by a trial wave function

$$\psi(\mathbf{r},t) = \psi(\mathbf{r},\mathbf{z}(t)). \quad (3)$$

Here,  $\mathbf{z}(t) = [z_1(t), z_2(t), \dots, z_d(t)]^\top \in \mathbb{C}^d$  is a set of  $d$  complex and time-dependent variational parameters, and the time evolution of the wave function is completely determined by them. In the framework of the variational approach, the mean-field energy functional of the system is given by the expectation value of the Hamilton operator

$$E(\mathbf{z}) = \left\langle \psi(\mathbf{r},\mathbf{z}) \left| -\Delta + V_{\text{ext}} + \frac{1}{2}(V_c + V_{\text{lr}}) \right| \psi(\mathbf{r},\mathbf{z}) \right\rangle, \quad (4)$$

where the factor 1/2 is included to avoid a double-counting of the two-particle interactions. In order to describe the dynamics of the system in the Hilbert subspace which is spanned by the variational ansatz (3), we apply the Dirac-Frenkel-McLachlan variational principle [36, 37]. This requires minimizing the norm of the difference between the left- and the right-hand side of the GPE (1),

$$I = \|\mathbf{i}\phi - \hat{H}\psi\|^2 \stackrel{!}{=} \min. \quad (5)$$

where, the arguments of the wave function  $\psi$  have been omitted for brevity. The quantity  $I$  is minimized with respect to  $\phi$  and  $\phi = \hat{\psi}$  is set afterwards which means that the GPE is solved within the Hilbert subspace of the variational ansatz with the least possible error. Proceeding from the complex variational parameters  $\mathbf{z}$  to their real and imaginary parts  $\mathbf{x} = (\mathbf{z}^r, \mathbf{z}^i)^\top \in \mathbb{R}^{2d}$ , it

was shown in Ref. [33] that minimizing Eq. (5) leads to the noncanonical Hamiltonian equations of motion

$$K(\mathbf{x}) \dot{\mathbf{x}} = -\frac{\partial E(\mathbf{x})}{\partial \mathbf{x}}, \quad (6)$$

where  $K_{mn} = 2\text{Im} \langle \frac{\partial \psi}{\partial x_m} | \frac{\partial \psi}{\partial x_n} \rangle$  and  $E(\mathbf{x}) = E(\mathbf{z}) |_{\mathbf{z} \rightarrow \mathbf{x}}$ .

In order to apply the variational approach to a BEC in a harmonic trap, a natural choice for the trial wave function (3) is a Gaussian one. Deviations from the pure Gaussian form which occur due to particle interactions can then be taken into account by using *coupled* Gaussian trial wave functions

$$\psi(\mathbf{r}, \mathbf{z}) = \sum_{k=1}^{N_g} g_k(\mathbf{r}, \mathbf{z}), \quad (7)$$

where we have omitted the explicit time-dependence of the variational parameters  $\mathbf{z}$  for brevity. Depending on the inherent symmetry of the physical system, we will choose one of the following forms in this paper:

$$g_k(\mathbf{r}, \mathbf{z}) = \exp(A_r^k r^2 + \gamma^k), \quad (8a)$$

$$g_k(\mathbf{r}, \mathbf{z}) = \exp(A_\rho^k \rho^2 + A_z^k z^2 + \gamma^k). \quad (8b)$$

Here, we use the complex variational parameters  $\mathbf{z} = (A_r^k, A_\rho^k, A_z^k, \gamma^k)^T$ : the parameters  $A_{r,\rho,z}^k$  determine the width of each Gaussian and  $\gamma^k$  are the norm and phase, respectively. Equation (8a) is an appropriate choice for the radially symmetrical system without DDI and Eq. (8b) for the dipolar system with cylindrical symmetry. We note that, because the total wave function is normalized to  $|\psi(\mathbf{r}, t)|^2 = 1$  and its global phase is free, the total number of independent variational parameters is reduced by one. Consequently, there remain  $d = 2N_g - 1$  degrees of freedom in case of the ansatz (8a) and  $d = 3N_g - 1$  in case of Eq. (8b). For the detailed application of the time-dependent variational approach, i. e. the evaluation of the energy functional (4) and the dynamical equations (6), we refer the reader to Ref. [38].

### C. Normal form expansion and TST

In the investigations of BECs, fixed points of the dynamical equations (6) are of special interest, because they correspond to stationary states of the system as, e. g., its ground or transition state. Just as important as the fixed points themselves are their local properties, since these determine the elementary excitations and the structure of the reaction channel. Within the lowest-order approximation to the condensate's dynamics, a possible approach to determine the elementary excitations are the Bogoliubov-de Gennes equations. The latter result from a linearization of the GPE (1) for small deviations from its ground state and yield the BEC's collective frequencies  $\pm\omega_i$ . The same can be obtained from the variational approach by linearizing the dynamical equations

(6) at a fixed point giving the finite set of frequencies  $(\pm\omega_1, \pm\omega_2, \dots, \pm\omega_d)$  [39, 40].

Beyond the linear approximation of the dynamics, we are, in this paper, also interested in the higher-order corrections. A systematic way to investigate the local fixed point properties to any desired order is a normal form expansion of the dynamical equations (6). This method has been described in detail in Ref. [33] and we will only discuss it here very briefly: The essential procedure to bring the noncanonical Hamiltonian system into its canonical normal form is based on a power series expansion of the energy functional (4) and the dynamical equations (6) at the respective fixed point. Successive Lie transforms which are performed order by order bring the system into its normal form. Furthermore, the corresponding generating function of the transformation is chosen in such a way that the resulting dynamical equations as well as the energy functional fulfill canonical equations, i. e. the normal form coordinates are canonical ones. Finally, the energy functional (4) in these coordinates serves as a classical Hamilton function. Using the multi-index notation  $\mathbf{x}^{\mathbf{m}} = x_1^{m_1} x_2^{m_2} \dots x_d^{m_d}$  and  $|\mathbf{m}| = m_1 + m_2 + \dots + m_d$ , the latter is a multivariate polynomial in action variables  $\mathbf{J}$ ,

$$H(\mathbf{J}) = \sum_{|\mathbf{m}|=0}^{\chi} \xi_{\mathbf{m}} \mathbf{J}^{\mathbf{m}}, \quad (9)$$

where  $\chi$  is the normal form order chosen and  $\xi_{\mathbf{m}}$  are the coefficients of the expansion. The zeroth-order coefficient  $\xi_{|\mathbf{m}|=0} = E_{\text{mf}}$  is the mean-field energy and those of first-order are the oscillation frequencies  $\xi_{|\mathbf{m}|=1} = \omega_i$  ( $i = 1, \dots, d$ ). The polynomial structure of Eq. (9) can always be obtained if the first-order coefficients of the expansion are rationally independent, i. e. the equation

$$\sum_{\mathbf{m}} n_{\mathbf{m}} \xi_{|\mathbf{m}|=1} = 0 \quad (10)$$

with  $n_{\mathbf{m}} \in \mathbb{Z}$  has only the trivial solution  $n_{\mathbf{m}} = 0$ . It is emphasized that the expansion coefficients  $\xi_{\mathbf{m}}$  in Eq. (9) contain the full information about the local dynamics at the fixed points.

In addition to the simple structure of Eq. (9) in normal form coordinates, a big advantage of this canonical Hamiltonian is that it allows one to apply all methods which are known from classical Hamiltonian mechanics. One important application is the field of TST [29–32] where reactions are described qualitatively and quantitatively that are mediated by a transition state in phase space: If  $J_1$  is the reaction coordinate, then the transition state is defined by  $J_1 = 0$  and the thermally averaged reaction rate is [30]

$$\Gamma = \frac{1}{2\pi\beta} \frac{\int dJ_2 \dots dJ_d \exp(-\beta H(0, J_2, \dots, J_d))}{\int dJ'_1 \dots dJ'_d \exp(-\beta H'(J'_1, \dots, J'_d))}. \quad (11)$$

Here,  $H$  is the normal form Hamiltonian of the system at its transition state,  $H'$  is the corresponding one at the ground state, and  $\beta = 1/k_{\text{B}}T$  is the inverse temperature.

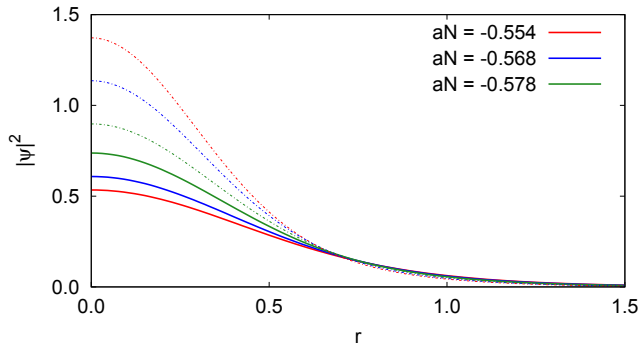


Figure 1. (Color online) Density distribution  $|\psi(\mathbf{r})|^2$  of the condensate in its ground (solid lines) and transition state (dash-dotted lines) at different values of the s-wave scattering length and for  $N_g = 2$  coupled Gaussians. Compared to the ground state, the transition state exhibits a higher density at the center of the trap and a lower density far away from it. With decreasing scattering length, the maximum density of the ground state increases, while that of the transition state decreases, and at the critical scattering length  $a_{\text{crit}}N = -0.579$  they match.

### III. APPLICATION TO BECS WITH SHORT- AND LONG-RANGE INTERACTION

#### A. BECs with short-range interaction

A BEC with short-range interaction is described by the GPE (1) with  $V_{\text{tr}} = 0$  and, as already mentioned above, we focus on a system that is confined in a spherically symmetrical trap  $V_{\text{ext}} = \mathbf{r}^2$ . Searching for fixed points of the corresponding dynamical equations (6) in the variational framework, one can find two stationary states above a critical scattering length  $a_{\text{crit}}$ , one of which corresponds to the ground state and the other is its transition state.

In Fig. 1, the density distributions  $|\psi(\mathbf{r})|^2$  of the ground (solid lines) and the transition state (dash-dotted lines) are shown for different values of the s-wave scattering length and  $N_g = 2$  coupled Gaussians. Compared to the ground state, the transition state in general exhibits a higher density at the center of the trap and a lower density far away from it. With decreasing scattering length, the density of the ground state increases, while that of the transition state decreases, and at the critical value  $a_{\text{crit}}N$  of the scattering length, the two states become identical. Because the interaction is attractive ( $aN < 0$ ) and the density distribution directly enters the contribution of the particle scattering, the transition state physically represents a highly attracting configuration of the condensate. More precisely, its physical interpretation is a density distribution on the edge of the BEC's collapse: For any higher (local) density, the attractive interaction would dominate the quantum pressure leading to the collapse of the condensate. Any lower density would result in an excited but stable BEC. This interpretation can be verified by actually calculating the dynamics of the BEC

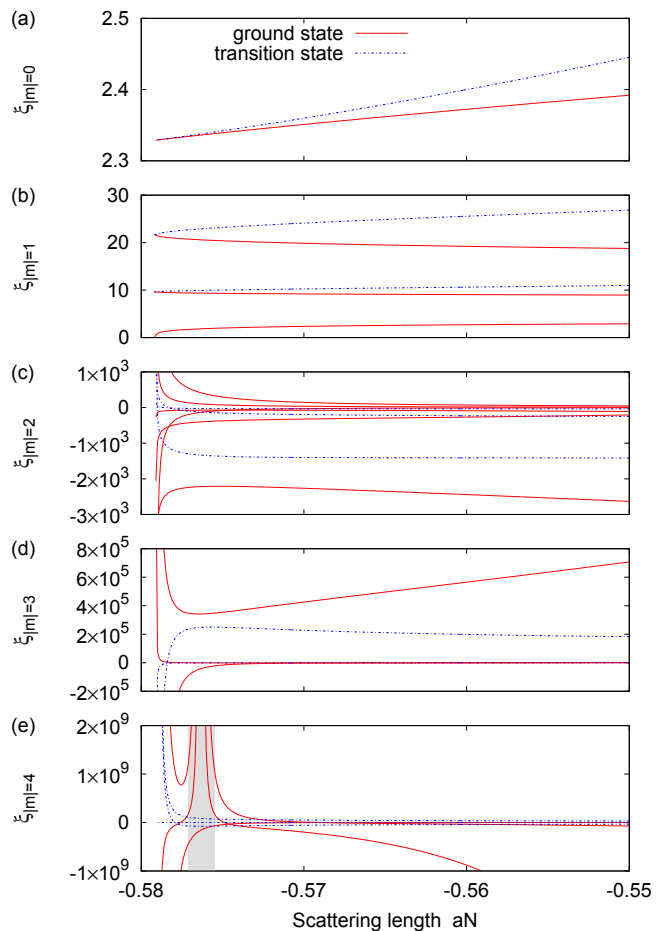


Figure 2. (Color online) Coefficients of the normal form expansion in different orders for an approximation of the condensate wave function with  $N_g = 2$  coupled Gaussian wave functions. (a) The zeroth-order coefficient is the mean-field energy ( $\xi_{|m|=0} = E_{\text{mf}}$ ) of the stationary state. (b) The first-order coefficients correspond to the eigenvalues of the linearized dynamical equations ( $\xi_{|m|=1} = \omega_i$ ,  $i = 1, \dots, d$ ) and describe the frequencies of the Bogoliubov quasi-particle modes. (c)–(e): Higher-order terms give corrections of the dynamics in the vicinity of the fixed points and they define the coupling strength of the single quasi-particle modes (only a selection is presented for the sake of clarity). The gray bar in (e) is intended to highlight the divergence of some coefficients (cf. Fig. 3).

[28, 41], which reveals its collapse in the center of the trap after the transition state has been crossed.

In Fig. 2 the normal form expansion coefficients which fully describe the local properties of the fixed points are shown for the ground and the transition state: The zeroth-order coefficients  $\xi_{|m|=0} = E_{\text{mf}}$  [see Fig. 2(a)] are the mean-field energies of the stationary states. The energetically lower one is the metastable ground state of the BEC and the other excited state is the transition state. For  $N_g = 2$ , both these states emerge together in a tangent bifurcation at the critical value  $a_{\text{crit}}N \approx -0.579$  of the scattering length, below which the condensate no

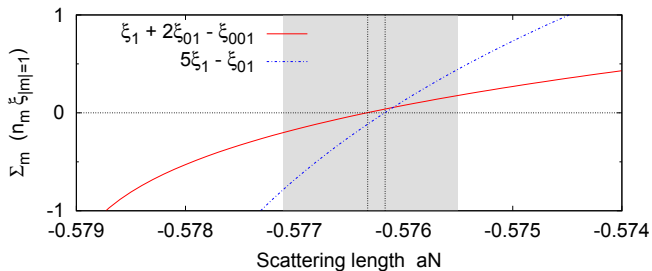


Figure 3. (Color online) Rational independence of the linear coefficients  $\xi_{|m|=1}$  for the same parameters as used in Fig. 2. Equation (10) is violated at  $aN = -0.57633$  where  $\xi_1 + 2\xi_{01} - \xi_{001} = 0$  and at  $aN = -0.57617$  where  $5\xi_1 - \xi_{01} = 0$ . The width of the gray area in the background is the same as in Fig. 2(e).

longer exists. Because the transition state has a higher energy than the ground state, an energy barrier has to be crossed in order to induce the BEC's collapse. The height of this barrier is given by the energy difference between the two states and it is high for large values of the scattering length. By contrast, it decreases when one approaches the critical value and vanishes there. Figure 2(b) shows the first-order coefficients ( $\xi_{|m|=1} = \omega_i$ ,  $i = 1, \dots, d$ ) of the local normal form which correspond to the frequencies of the Bogoliubov quasi-particle modes. All these coefficients show a smooth dependence on the scattering length. At the latter's critical value, two of them merge in each case.

For larger deviations of the system from one of the fixed points, higher-order contributions become important which are shown in Figs. 2(c)–(e). All three figures show that the higher-order corrections have quite large numerical values (on the order of up to  $10^9$ ) as compared to the oscillation frequencies (on the order of  $10^1$ ), and that they diverge at the critical scattering length  $a_{\text{crit}}N$ . This gives rise to the expectation that the corrections can have significant influence on the reaction rate, because their contribution becomes important in the vicinity of the critical scattering length.

We note that the pole occurring in some fourth-order coupling terms [highlighted by the gray background in Fig. 2(e)] is a resonance in the normal form procedure. As shown in Fig. 3, there are two nearby values of the scattering length  $aN = -0.57633$  and  $aN = -0.57617$ , where the frequencies become rationally dependent, i. e. Eq. (10) is violated. In this case there is a strong mode coupling of the condensate's higher harmonics in the respective order, which leads to the failure of the normal form procedure as described in Ref. [33].

According to the variational ansatz (3), where the number  $N_g$  of coupled wave functions appears as a free parameter, one expects that all the results depend on this parameter. Therefore, an important topic is the convergence of the normal form when the number of coupled Gaussians is varied. For the following investigations of

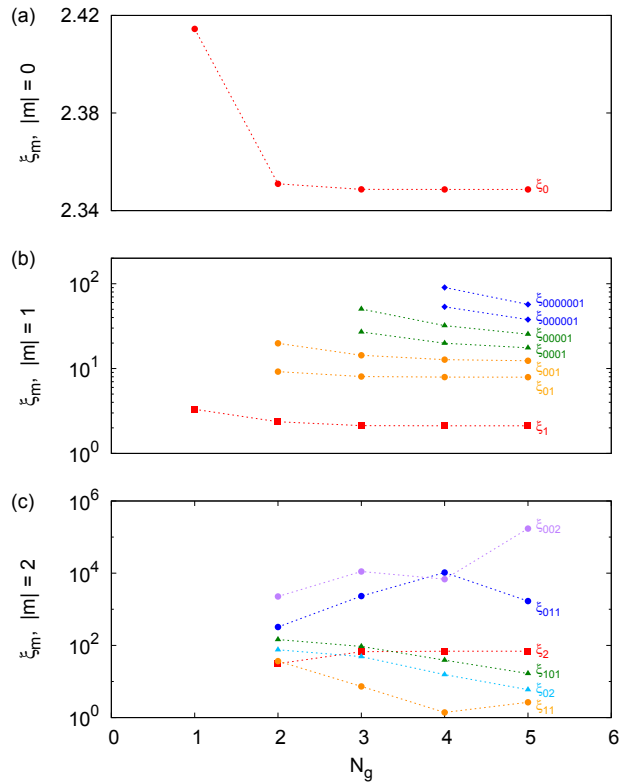


Figure 4. (Color online) Behavior of the normal form expansion coefficients for a trial wave function in Eq. (3) consisting of a different number  $N_g$  of coupled Gaussians. The scattering length is chosen as  $aN = -0.57$ . In (a), the zeroth-order coefficient (fixed point energy) converges very fast. The first-order contributions (Bogoliubov quasi-particle frequencies) in (b) show a monotonic decrease. The lowest terms converge fast while the higher terms are not yet converged for  $N_g = 5$ . In the higher-order expansion coefficients (c), one observes the convergence of some coupling terms, while some others are not converged yet. [Note that only a selection of coupling terms with a typical behavior is presented in (c) due to the huge amount of such terms.]

the single expansion coefficients, we will use a simplified notation in which each  $\mathbf{m}$ -index in Eq. (9) is only displayed up to its last nonzero entry and successive zeros are neglected (e. g. the expansion coefficient  $\xi_{021000}$  will be displayed as  $\xi_{021}$ ). This makes it easy to compare expansion coefficients which result from different variational approaches in which the dimension of  $\mathbf{m}$  depends on the number  $N_g$  of coupled Gaussian wave functions.

In Fig. 4, we present the convergence behavior of a selection of coefficients in dependence on the number  $N_g$  of coupled Gaussian trial wave functions. The zeroth-order coefficient  $\xi_0$  in Fig. 4(a), i. e. the fixed point energy, converges very fast. The most significant correction is observed when one increases from  $N_g = 1$  to  $N_g = 2$ . In the last step shown ( $N_g = 4$  to  $N_g = 5$ ) the relative correction is about  $4.4 \times 10^{-7}$ , so that this value can be treated as converged. The analogous behavior of the first-order

coefficients is shown in Fig. 4(b). As already discussed in Sec. II C, the number of degrees of freedom is  $d = 2N_g - 1$ . Therefore, two more terms occur with each increase of  $N_g$  which are indicated by the same symbols in this figure. For a small number of coupled Gaussian wave functions, the corresponding coefficients are small and they correspond to low-frequency oscillation modes (e. g. the lowest coefficient is the frequency of the BEC's breathing mode). The lowest terms only change marginally when the number  $N_g$  of coupled Gaussians is increased, thus convergence is observed early. For the terms that correspond to more complicated higher-frequency oscillation modes, the corrections become larger, and they are still significant for  $N_g = 5$ . In this case, even more advanced trial wave functions will be required to observe convergence. It is obvious throughout that the single coefficients decrease monotonically with larger values  $N_g$ , so that one always expects the numerical results to overestimate the true values.

Finally, we present in Fig. 4(c) the behavior of a selection of second-order normal form contributions which correspond to the lowest-order coupling terms of the condensate oscillation modes: It can be seen that the convergence of these coupling terms is not as simple as that of the zeroth- and first-order terms. The red squares in Fig. 4(c) exemplarily show a converging coupling coefficient. However, one can also observe other coefficients which exhibit throughout a monotonic decrease (triangles) or a nonmonotonic behavior (dots) and which are not yet converged.

As already mentioned above, the knowledge of the ground and the transition state of the BEC as well as their local properties allows one to calculate the condensate's thermal decay rate by applying TST. Therefore, a normal form expansion is performed at the ground and the transition state of the condensate which yields two normal form Hamiltonians  $H$  and  $H'$ . The decay rate is, finally, given by Eq. (11) where the integrals are evaluated numerically via a Monte Carlo integration. In the following, we present results for an exemplary BEC of  $N = 1000$   $^{87}\text{Rb}$  atoms in a trap of strength  $\omega = 2\pi \times 100$  Hz. Figure 5(a) shows the decay rate in dependence on the scattering length at a temperature of  $T = 24$  nK for  $N_g = 2$  coupled Gaussians. With decreasing scattering length, the decay rate significantly increases. It has its largest values close to  $a_{\text{crit}}N$  where the energy barrier is small. The drop of the first-order rate ( $\chi = 1$ ) to zero at  $a_{\text{crit}}N$  is not physical, since the barrier vanishes there and the rate should strongly increase. This tendency is correctly reproduced by the higher-order approximations ( $\chi > 1$ ) of the transition state. Furthermore, it can be seen that corrections to the decay rate are significant near the critical scattering length, where better approximations of the transition state yield higher reaction rates. We note that the peak in the fourth-order approximation at  $aN \approx -0.5763$  is caused by the numerical resonance in the normal form coefficients that has already been discussed above [cf. Fig. 2(e)] and is not

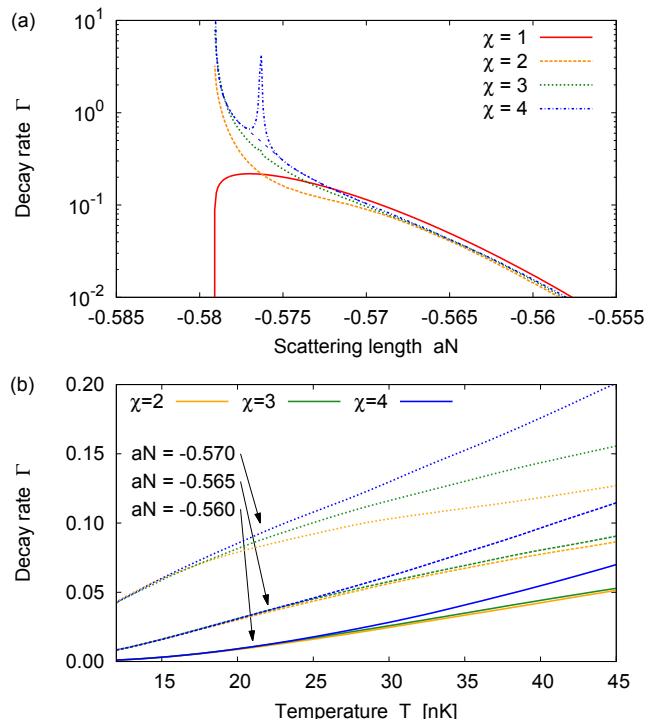


Figure 5. (Color online) Decay rate of the thermally induced coherent collapse of a BEC consisting of  $N = 1000$   $^{87}\text{Rb}$  atoms in a trap with frequency  $\omega = 2\pi \times 100$  Hz and at a temperature of  $T = 24$  nK. The calculations have been performed for  $N_g = 2$  coupled wave functions. (a) The decay rate increases with decreasing scattering length and it reaches its highest values close to the critical value  $a_{\text{crit}}N$ . Also corrections of the higher-order normal form expansions become more important in this region. (b) The decay rate also increases with the temperature. Higher normal form orders predict higher decay rates throughout. At low temperatures, the corrections are small and already the second-order ( $\chi = 2$ ) approximation of the transition state can be sufficient. By contrast, higher normal form orders give significant corrections at higher temperatures.

physical. The expected physical behavior is sketched by a dashed line.

In Fig. 5(b), the decay rate is presented in dependence of the condensate temperature  $T$ . Throughout, one finds that higher normal form approximations are less important at low temperatures and very important at higher temperatures. Vice versa, the behavior of the decay rate in Fig. 5(b) can be used in order to estimate the temperature regime up to which a certain approximation will yield good results.

## B. BECs with long-range dipolar interaction

Beyond BECs with short-range scattering interaction, also condensates with long-range and anisotropic DDI have been realized experimentally [4–6]. The investigation of the thermally induced coherent collapse in dipo-

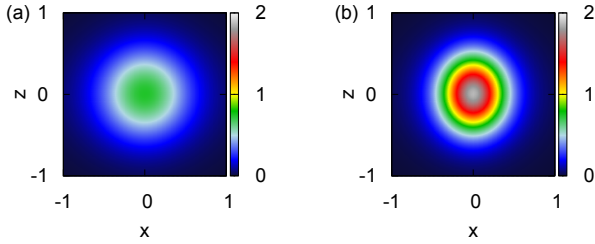


Figure 6. (Color online) Density distribution  $|\psi(\mathbf{r})|^2$  (cut through the  $x$ - $z$ -plane) of a dipolar BEC calculated with  $N_g = 2$  coupled Gaussian wave functions at a scattering length  $aN = -0.47$ . The density distribution of the ground state (a) is slightly extended more in the radial direction than in  $z$ -direction. By contrast, the density distribution of the transition state (b) is more extended in  $z$ -direction. Moreover, it exhibits a highly increased density in the center of the trap as compared to the ground state.

lar BECs has already been performed within the lowest-order approximation of the transition state [27, 28]. Therein, additional transition states emerged in bifurcations which gave rise to the expectation of a symmetry-breaking thermally induced collapse at certain physical parameters. It is not the scope of this paper to investigate this symmetry-breaking collapse scenario in more detail. Instead, we focus on the effects of higher-order normal form approximations of the transition state [35].

We therefore numerically solve the GPE (1) with the variational ansatz (8b) and apply the normal form procedure as described in Ref. [33]. We consider an external trap aspect ratio  $\lambda = 2$ , where the dipolar BEC shows a conventional density distribution and where only a single transition state with cylindrical symmetry exists [28]. The strength of the DDI in Eq. (2) is determined by the coefficient  $a_{dd}N$  and it depends on the particle number. For an exemplary  $^{52}\text{Cr}$  condensate in a trap with frequency  $\omega_\rho = 2\pi \times 100$  Hz, the parameter  $a_{dd}$  has a value  $a_{dd} \approx 0.0034$ , and in case of  $^{164}\text{Dy}$  the value is  $a_{dd} \approx 0.0536$ . For the following calculations, we use a model condensate with  $a_{dd}N = 1$  which represents each of these dipolar condensates with a respective particle number.

The physical meaning of the transition state in dipolar BECs is the same as in the case without long-range interaction as discussed in Sec. III A. However, because of the anisotropy of the DDI, the extensions of the atomic cloud in  $\rho$ - and  $z$ -direction differ (see Fig. 6): Due to the interplay between the external trap with the DDI which prefers an alignment of the dipoles in head-to-tail configuration, the ground state in Fig. 6(a) only has a slightly larger extension in the radial than in  $z$ -direction. By contrast, the density distribution of the transition state in Fig. 6(b) is more extended in  $z$ -direction and it exhibits a highly increased density in the center of the trap. Due to these two effects, the transition state corresponds to a

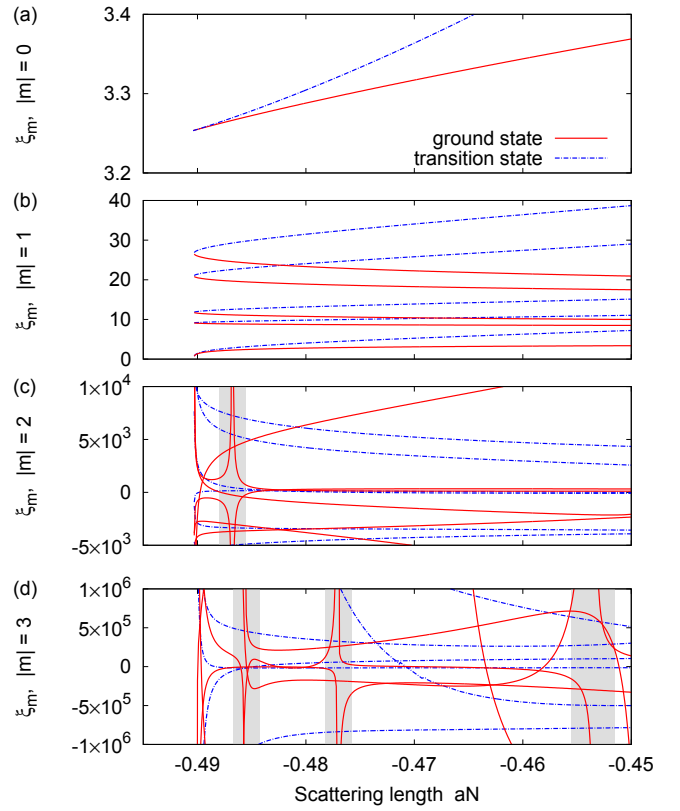


Figure 7. (Color online) Coefficients of the normal form expansion in different orders for a dipolar condensate with  $N_g = 2$  coupled Gaussian wave functions. As in Fig. 2, the fixed-point energies (a) of the ground and the transition state as well as the Bogoliubov eigenfrequencies (b) show a smooth behavior and the respective values merge at the critical scattering length  $a_{\text{crit}}N = -0.4903$ . The coupling coefficients (c),(d) of the collective oscillation modes show poles at different values of the scattering length  $a$  (highlighted by the gray bars), whose number increases with higher normal form orders. (Again, only a selection of the coefficients with a typical behavior is presented for the sake of clarity).

highly attractive configuration of the interacting bosons. As in the case without long-range interaction, this stationary state represents the condensate at the edge of the collapse. Any locally higher density and, with it, a higher attraction between the particles would lead to the collapse of the condensate.

Again, the full information about the condensate's local dynamics is reflected by the normal form coefficients which are shown in Fig. 7, and also the interpretation of the individual orders of the expansion is the same as in Sec. III A. The energy eigenvalues [see Fig. 7(a)] and the frequencies of elementary excitations [see Fig. 7(b)] show a smooth dependence on the scattering length and they merge at the latter's critical value. Also, we observe that the coupling terms of the modes [see a selection in Figs. 7(c),(d)] are important because they have numerically large values. What is different is that a resonance can already be found in the second order  $|m| = 2$  where

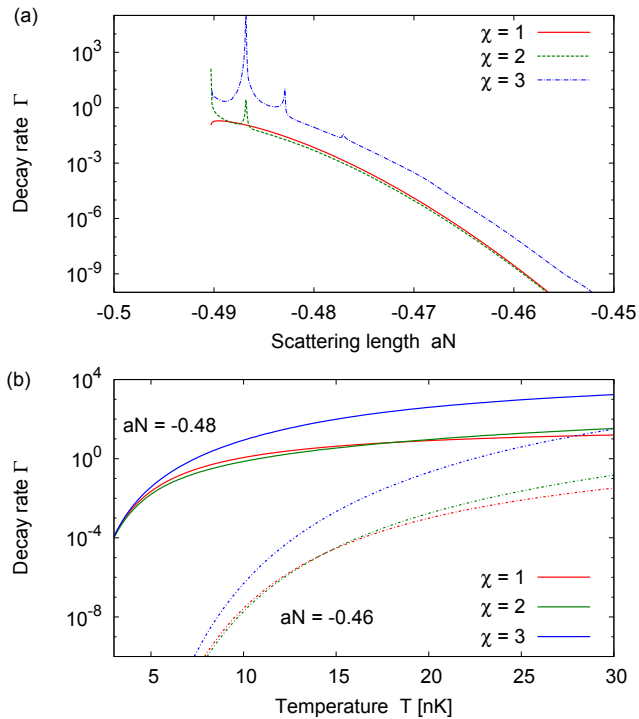


Figure 8. (Color online) (a) Thermal decay rate of a dipolar BEC in dependence on the scattering length and for different normal form orders  $\chi$  (parameters:  $\beta = 200$ ,  $N_g = 2$ ). (b) Decay rate in dependence on the temperature.

some coefficients diverge (highlighted by a gray bar in the background of the plot). The reason for this earlier occurrence of resonances compared to that in Fig. 2 is, here, that the variational approach (8b) exhibits more degrees of freedom than the ansatz (8a). As a consequence, there exist more possible oscillation modes that can couple according to Eq. (10), which also leads to three more resonances in the third normal form order in Fig. 7(c). Analogously to the case discussed in Fig. 3, also each of these resonances can be identified with a certain mode coupling of higher harmonics in the dipolar BEC. However, a detailed investigation of these mode couplings goes beyond the scope of this paper and we refer the reader to Ref. [35] for further studies including the effect of varying external parameters on the resonances.

In Fig. 8, the thermal decay rate is shown in dependence on the scattering length and the temperature  $T$ . According to Fig. 8(a) higher-order corrections are, again, important: The second-order decay rate ( $\chi = 2$ ) gives only small corrections to the decay rate compared to the first order ( $\chi = 1$ ). However, importantly, the second order correctly reproduces an increasing decay rate when one approaches the critical scattering length. For the given temperature, the third-order normal form predicts an increased reaction rate over the whole range of the scattering length of about one order of magnitude. Again, we note that the single peaks are a consequence of the resonances shown in Fig. 7 and that they are not

physical. As presented in Fig. 8(b), the higher-order corrections to the decay rate are again important at high temperatures, whereas the first-order approximation of the transition state already is appropriate for small temperatures.

#### IV. CONCLUSION

In this paper, we have investigated the properties of the ground and transition state in BECs with short- and long-range interaction. In both systems, we have discussed the transition state as a certain density distribution of the atomic cloud that typically exhibits a locally increased density in the center of the trap as compared to the ground state. Higher-order normal form approximations to the local dynamics of the condensate in the vicinity of their fixed points turned out to be important throughout, because their large numerical values induce significant corrections already at small deviations from the stationary states. As a general tendency, we observed that low-order normal form contributions converge quite fast when the trial wave function is improved, while higher-order corrections show slower convergence.

Calculating the decay rate of the condensates by applying TST, we observed significant corrections especially close to the critical value of the scattering length where the attraction dominates in the system. Higher-order normal form approximations are capable of reproducing the physically expected behavior of a monotonically increasing reaction rate when the critical scattering length is approached. In general, the reaction rates within higher-order approximations are dramatically increased compared to the usual harmonic approximation of the transition state, which gives rise to the expectation that the decay mechanism of the thermally induced coherent collapse can play an even more important role than estimated in previous investigations [28].

Finally, our investigations revealed that resonances in the normal form procedure become more and more important in higher-order approximations and for a large number of degrees of freedom. To appropriately treat these resonances, the normal form expansions presented in Ref. [33] need to be adapted to this situation which is currently work in progress. Another way to circumvent divergences in the normal form coefficients could be the application of uniform approximations [27] to the Hamiltonian by which bifurcations in the transition state have already been handled successfully.

- 
- [1] M. H. Anderson, J. R. Ensher, M. R. Matthews, C. E. Wieman, and E. A. Cornell, *Science* **269**, 198 (1995).
- [2] C. C. Bradley, C. A. Sackett, J. J. Tollett, and R. G. Hulet, *Phys. Rev. Lett.* **75**, 1687 (1995).
- [3] K. B. Davis, M. O. Mewes, M. R. Andrews, N. J. van Druten, D. S. Durfee, D. M. Kurn, and W. Ketterle, *Phys. Rev. Lett.* **75**, 3969 (1995).
- [4] A. Griesmaier, J. Werner, S. Hensler, J. Stuhler, and T. Pfau, *Phys. Rev. Lett.* **94**, 160401 (2005).
- [5] M. Lu, N. Q. Burdick, S. H. Youn, and B. L. Lev, *Phys. Rev. Lett.* **107**, 190401 (2011).
- [6] K. Aikawa, A. Frisch, M. Mark, S. Baier, A. Rietzler, R. Grimm, and F. Ferlaino, *Phys. Rev. Lett.* **108**, 210401 (2012).
- [7] P. Pedri and L. Santos, *Phys. Rev. Lett.* **95**, 200404 (2005).
- [8] R. Nath, P. Pedri, and L. Santos, *Phys. Rev. Lett.* **102**, 050401 (2009).
- [9] I. Tikhonenkov, B. A. Malomed, and A. Vardi, *Phys. Rev. Lett.* **100**, 090406 (2008).
- [10] O. Dutta and P. Meystre, *Phys. Rev. A* **75**, 053604 (2007).
- [11] S. Ronen, D. C. E. Bortolotti, and J. L. Bohn, *Phys. Rev. Lett.* **98**, 030406 (2007).
- [12] K. Góral, K. Rzazewski, and T. Pfau, *Phys. Rev. A* **61**, 051601 (2000).
- [13] T. Koch, T. Lahaye, J. Metz, B. Fröhlich, A. Griesmaier, and T. Pfau, *Nat. Phys.* **4**, 218 (2008).
- [14] L. Santos, G. V. Shlyapnikov, P. Zoller, and M. Lewenstein, *Phys. Rev. Lett.* **85**, 1791 (2000).
- [15] K. Góral and L. Santos, *Phys. Rev. A* **66**, 023613 (2002).
- [16] L. Santos, G. V. Shlyapnikov, and M. Lewenstein, *Phys. Rev. Lett.* **90**, 250403 (2003).
- [17] R. M. Wilson, S. Ronen, J. L. Bohn, and H. Pu, *Phys. Rev. Lett.* **100**, 245302 (2008).
- [18] J. Metz, T. Lahaye, B. Fröhlich, A. Griesmaier, T. Pfau, H. Saito, Y. Kawaguchi, and M. Ueda, *New J. Phys.* **11**, 055032 (2009).
- [19] T. Lahaye, J. Metz, B. Fröhlich, T. Koch, M. Meister, A. Griesmaier, T. Pfau, H. Saito, Y. Kawaguchi, and M. Ueda, *Phys. Rev. Lett.* **101**, 080401 (2008).
- [20] H. T. C. Stoof, *J. Stat. Phys.* **87**, 1353 (1997).
- [21] K. Marquardt, P. Wieland, R. Häfner, H. Cartarius, J. Main, and G. Wunner, *Phys. Rev. A* **86**, 063629 (2012).
- [22] S. Hensler, J. Werner, A. Griesmaier, P. O. Schmidt, A. Görlitz, T. Pfau, K. Rzazewski, and S. Giovanazzi, *Appl. Phys. B* **77** (2003).
- [23] C. Huepe, S. Métens, G. Dewel, P. Borckmans, and M. E. Brachet, *Phys. Rev. Lett.* **82**, 1616 (1999).
- [24] C. Huepe, L. S. Tuckerman, S. Métens, and M. E. Brachet, *Phys. Rev. A* **68**, 023609 (2003).
- [25] A. Junginger, J. Main, G. Wunner, and M. Dorwarth, *J. Phys. A: Math. Theor.* **45**, 155201 (2012).
- [26] A. Junginger, M. Dorwarth, J. Main, and G. Wunner, *J. Phys. A: Math. Theor.* **45**, 155202 (2012).
- [27] A. Junginger, J. Main, G. Wunner, and T. Bartsch, *Phys. Rev. A* **86**, 023632 (2012).
- [28] A. Junginger, M. Kreibich, J. Main, and G. Wunner, *Phys. Rev. A* **88**, 043617 (2013).
- [29] P. Pechukas, *Ann. Rev. Phys. Chem.* **32**, 159 (1981).
- [30] P. Hänggi, P. Talkner, and M. Borkovec, *Rev. Mod. Phys.* **62**, 251 (1990).
- [31] D. G. Truhlar, B. C. Garrett, and S. J. Klippenstein, *J. Phys. Chem.* **100**, 12771 (1996).
- [32] H. Waalkens, R. Schubert, and S. Wiggins, *Nonlinearity* **21**, R1 (2008).
- [33] A. Junginger, J. Main, and G. Wunner, arXiv:1409.0673 (2014).
- [34] T. Schaller, *Normalformentwicklungen für kugelsymmetrische Bose-Einstein-Kondensate mit gekoppelten Gauß-funktionen*, Bachelor thesis, Universität Stuttgart (2014), [http://www.itp1.uni-stuttgart.de/publikationen/abschlussarbeiten/schaller\\_bachelor\\_2014.pdf](http://www.itp1.uni-stuttgart.de/publikationen/abschlussarbeiten/schaller_bachelor_2014.pdf).
- [35] G. Hämmerling, *Normal form expansions for dipolar Bose-Einstein condensates with coupled Gaussian wave functions*, Bachelor thesis, Universität Stuttgart (2014), [http://www.itp1.uni-stuttgart.de/publikationen/abschlussarbeiten/haemmerling\\_bachelor\\_2014.pdf](http://www.itp1.uni-stuttgart.de/publikationen/abschlussarbeiten/haemmerling_bachelor_2014.pdf).
- [36] J. Frenkel, *Wave mechanics. Advanced General Theory* (Clarendon Press, Oxford, 1934).
- [37] A. D. McLachlan, *Mol. Phys.* **8**, 39 (1964).
- [38] S. Rau, J. Main, and G. Wunner, *Phys. Rev. A* **82**, 023610 (2010).
- [39] M. Kreibich, J. Main, and G. Wunner, *J. Phys. B: At. Mol. Opt. Phys.* **46**, 045302 (2013).
- [40] M. Kreibich, J. Main, and G. Wunner, *Phys. Rev. A* **86**, 013608 (2012).
- [41] H. Cartarius, T. Fabčić, J. Main, and G. Wunner, *Phys. Rev. A* **78**, 013615 (2008).